

REGULAR ARTICLE



Threshold Conditions for 1-D Model of Laser with Partial Active Region

S.S. Herasymov¹, O.S. Hnatenko^{1,*} , S.V. Dukhopelnykov^{2,3,4}, D.O. Herasymova²

¹ Kharkiv National University of Radio Electronics, 61166 Kharkiv, Ukraine,

² Institute of Radio-Physics and Electronics NASU, 61085 Kharkiv, Ukraine

³ V.N. Karazin Kharkiv National University, 61022 Kharkiv, Ukraine

⁴ Institut d'Electronique et de Technologies du numéRique - UMR 6164, Université de Rennes, 35042 Rennes, France

(Received 20 May 2024; revised manuscript received 15 August 2024; published online 27 August 2024)

The threshold conditions for a layered plane-parallel laser model consisting of a cavity filled with a gain material are considered in this work. The lasing modes can be viewed as natural modes with purely real-valued frequencies, in other words, the solutions of the source-free Maxwell equations. To investigate the mode-specific emission frequencies and the threshold gain index values, we apply the Lasing Eigenvalue Problem approach. By using this approach, we look for the mentioned values as the components of two-component eigenvalues of a specific time-harmonic electromagnetic boundary problem where the active region is presented and characterized by an imaginary part of the gain material refractive index. The obtained results clarify the effect of the gain material choice. Besides, the approximate expression for the gain per the normalized wavelength for the on-threshold modes was obtained and showed agreement with lasing mode trajectories for varying relative active region thickness. This analysis can be useful in the optimization of the laser performance due to achieving of lower threshold leading to larger output power which is crucial for e.g. industrial and military laser device applications.

Keywords: Laser mode, Threshold gain, Eigenproblem, Microcavity, Active region.

DOI: [10.21272/jnep.16\(4\).04033](https://doi.org/10.21272/jnep.16(4).04033)

PACS numbers: 03.50.De, 41.90.e, 42.55.Rz, 42.62.Cf

1. INTRODUCTION

Since the invention of laser last century, these devices have been greatly developed along several different configurations of the resonant cavities [1-5]. To achieve the lasing, these cavities must contain the active regions, filled in with a gain material. The latter are the doped crystalline or semiconductor or polymeric materials that can be optically or electrically pumped to produce laser light through the stimulated emission. The choice of the gain material and its specific characteristics significantly influence the performance and suitability of the laser for various applications.

Some of the commonly used gain materials in the fiber and solid-state lasers include crystals, ceramics and glasses doped with the rare earth or transition metal ions. Common doping elements are Er, Yb, Nd, Tm, Ho, Ti and Cr [6-8]. The active region is typically embedded in a solid-state matrix. The matrix provides the structural integrity necessary for maintaining the alignment of the active ions and the optical properties required for lasing. High thermal conductivity is often desirable to dissipate the heat generated during the laser operation, preventing thermal damage to the gain material. The choice of the active region host material and dopants defines the possible emission range of the laser, while the exact wavelength value is dictated by the cavity configuration.

Among these, the Neodymium and Erbium-doped Yttrium Aluminum Garnet (Nd:YAG and Er:YAG) lasers stand out as a prominent and versatile technology. The Er:YAG crystal-based laser can generate high peak power pulses and operate at the wavelength of around 2940 nm, that is close to the absorption peak of water. It makes them highly efficient in dermatology, dentistry, and ophthalmology, as it is safe for the eyes. Crystal's broad absorption band in the near-infrared region allows efficient pumping using a variety of sources. Er:YAG lasers offer tunable output across the mid-infrared spectrum, enabling tailored emission for specific needs, such as spectroscopy and medical diagnostics. Meanwhile, the Nd:YAG crystal exhibits excellent optical properties, including a broad absorption spectrum and high thermal conductivity [9, 10]. These features contribute to the laser's ability to generate intense and coherent light. The classic Nd:YAG laser operating wavelength, typically in the infrared range of around 1064 nm, is well-suited for numerous industrial applications, including material processing, welding, and cutting [11-16]. In the medical field, Nd:YAG lasers find applications in dermatology, ophthalmology, and surgery, showcasing their precision and versatility. Furthermore, Nd:YAG lasers are instrumental in scientific research, particularly in spectroscopy and experimental physics [17-19]. As the demand for high-power and efficient lasers grows, Nd:YAG lasers remain at

* Correspondence e-mail: oleksandr.hnatenko@nure.ua



the forefront of solid-state laser technologies, driving innovation across various industries. Both described materials are suitable for laser diode pump at the pump wavelength 980 nm for Er-doped medium and 808 nm for Nd-doped.

In the works [20-22], we have investigated the Nd:YAG SSL setup from the experimental point of view; now we will consider a simplified configuration (reduced to a 1-D form), sketched in Fig.1, using the mathematical modeling tools. This work builds, in part, on the preceding conference paper [23] that has been significantly extended with new results.

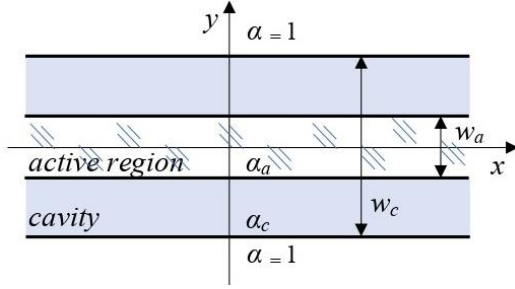


Fig. 1 – Sketches of the 1-D model of microcavity with partial active region in the free space environment

Micro lasers have attracted significant interest due to their compact size, low power consumption, and potential for integration into various photonic systems. The application areas involve optical sensing, portable electronics, biomedicine, defense and communication [24-28].

Within the laser design, it is essential to comprehend the gain threshold conditions. The lasing phenomenon in micro- and nanocavities involves multiple physical mechanisms, presenting a complex undertaking. However, to access the threshold conditions, all non-electromagnetic effects can be neglected, and the modeling problem can be reduced to the analysis of linear set of source-free Maxwell equations with exact boundary and radiation conditions. Such a framework is called the Lasing Eigenvalue Problem (LEP) approach, detailed in [29, 30]. The LEP approach allows us to look for mode threshold values of the gain index along with the mode emission frequencies. More precisely, both quantities form the ordered mode-specific two-component eigenvalues, (wavelength, threshold gain). Since the 2000s, LEP has been implemented for the analysis of threshold conditions in several models of micro and nanolasers, including the plasmonic ones with the noble-metal and patterned-graphene resonant elements – see [31-34].

In general, advancements in modeling and optimization in optical systems and high-power laser technologies can be found in [35-40].

In this paper, we analyze the thresholds conditions, from electromagnetic point of view, for the modes of the 1-D cavity in the free space, equipped with partial active region made of the gain crystals by using the mentioned eigenvalue problem.

2. EIGENVALUE PROBLEM FORMULATION

At the stationary emission threshold, the lasing modes can be viewed as natural modes with purely

real-valued frequencies, meaning they are the source-free Maxwell equations solutions with the time dependence $e^{-i\omega t}$, where $\omega > 0$ is the unknown cyclic frequency. In Fig. 1, we schematically present the considered 1-dimensional configuration of the layered dielectric cavity with a partial active region. The active material layer of the thickness w_a is placed inside the cavity of the thickness w_c . The relative dielectric permittivity of gain material is assumed a complex value, $\varepsilon_a = \varepsilon'_a + i\varepsilon''_a$ while all materials are nonmagnetic. As it is traditional in laser science, the gain material complex refractive index is introduced as $\nu = \sqrt{\varepsilon_a} = \alpha_a - i\gamma$, with a negative imaginary part. The real part of the refractive index, $\alpha_a > 0$, is assumed known while the imaginary part, $\gamma > 0$, is the unknown gain index threshold value. The relative dielectric permittivity of the passive part of the cavity is real value, $\varepsilon_c = \varepsilon'_c = \alpha_c^2$.

Assuming that the electromagnetic field does not vary along the x and z axes, we can characterize it using a scalar function E , representing the E_z field component. Off the layer boundaries, this function is required to satisfy the Helmholtz equation,

$$[\Delta + k^2 \nu^2(y)]E(y) = 0, \quad (1)$$

where $k = \omega/c$ is the wavenumber in the free space and piece-constant function $\nu(y)$ takes values α_c or ν inside the cavity and 1 out of it. The field tangential components must be continuous across the layer interfaces and obey the outgoing wave (1-D Sommerfeld) radiation condition at infinity ($|y| \rightarrow \infty$).

Furthermore, the uniform distribution of material gain across the active region layer, with no dependence on the frequency is assumed. It should be noted that, in reality, the gain index of any active-region material is a function of the wavelength, typically shaped as a Lorentzian with a material-specific central wavelength (say, 1064 nm for Nd:YAG and 2940 nm for Er:YAG). However, neglecting the gain dispersion makes the further analysis more straightforward and simplifies the comparison of the mode thresholds.

Taking into account the solutions without external sources for this boundary-value problem, within the LEP approach, we aim to identify its eigenvalues as a discrete set of pairs of real numbers, denoted as (κ_n, γ_n) . Here, the first one is the normalized lasing mode frequency $\kappa = kw_c$, while the second is the associated threshold value of the active region gain index. Note that for the Fabry-Perot cavity descriptions, the threshold gain is frequently characterized with the gain per unit length, $g = k\gamma$. However, this product is not a convenient quantity in arbitrary configurations; therefore, we believe that these two quantities should not be blended together.

3. FREE-SPACE CAVITY WITH PARTIAL ACTIVE REGION: COMPARISON OF TWO MATERIALS

In the simplest configuration depicted in Fig. 1, namely a dielectric slab microcavity (Fabry-Perot etalon) with a symmetrically positioned active region layer, the 1D LEP can be reduced to two independent equations [22]. These equations describe the symmetric and anti-symmetric modes, respectively,

$$\Phi(\kappa, \gamma) = e^{-i\kappa(\alpha_c - i\gamma)(w_a/w_c)} \pm \frac{R_c e^{i\kappa(\alpha_c - i\gamma)(w_a/w_c)} + R_a}{1 + e^{i\kappa(\alpha_c - i\gamma)(w_a/w_c)} R_c R_a} = 0, \quad (2)$$

where

$$R_a = i\gamma(2\alpha_c - i\gamma)^{-1}, \quad R_c = (\alpha_c - 1)(\alpha_c + 1)^{-1} \quad (3)$$

The zeros of (2) can be found using a gradient-search iterative algorithm. As the initial-guess values, one can use the approximate expressions established in [22],

$$\kappa_m \approx \frac{\pi(m+1)}{\alpha_c}, \quad \gamma_m \approx \frac{\ln[(\alpha_c + 1)/(\alpha_c - 1)]}{\kappa_m (w_a/w_c)}, \quad (4)$$

$m = 0, 1, 2, \dots$

which turn into accurate expressions in the case of the fully active flat layer, $w_a/w_c = 1$.

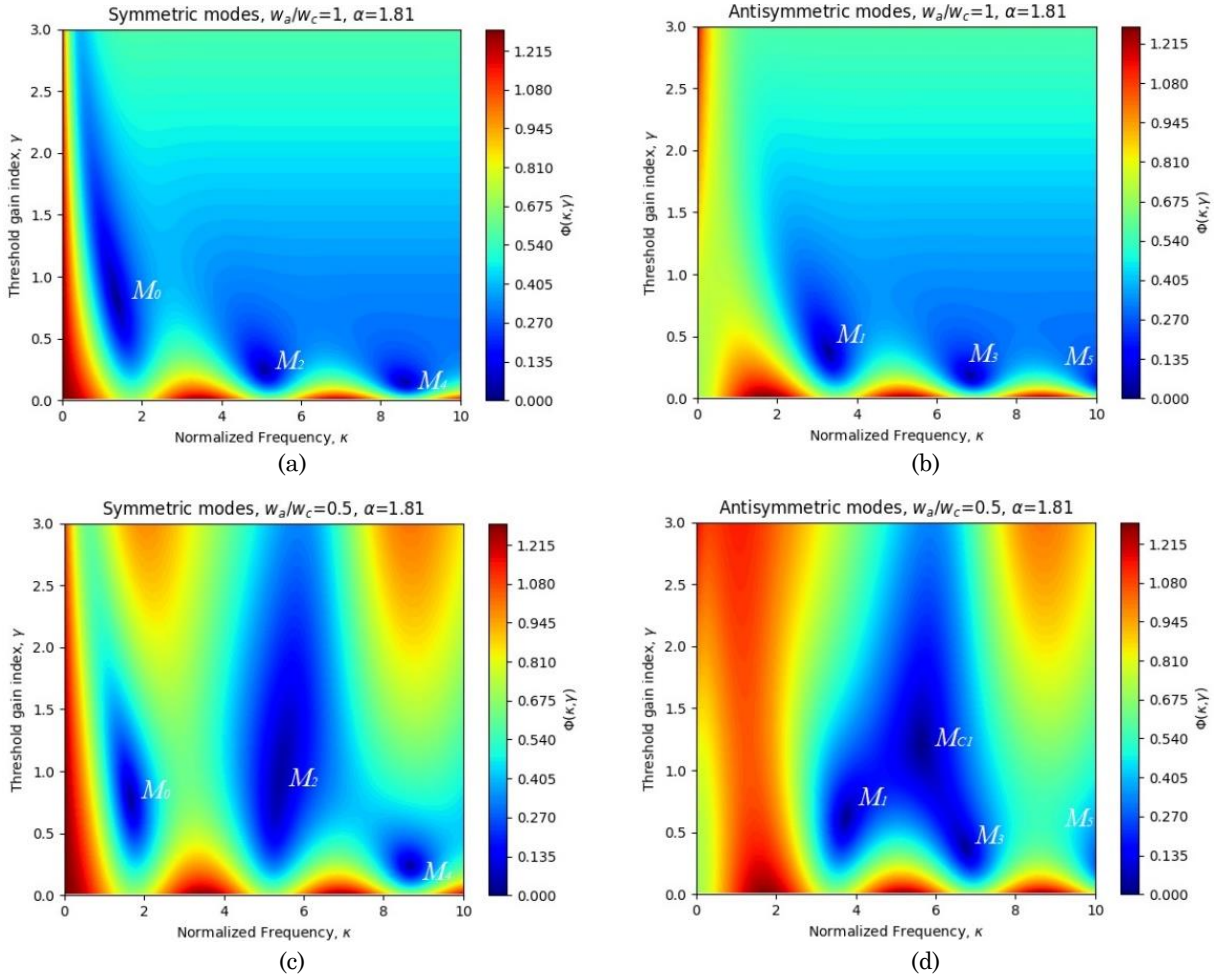
However, as we have found, even more accurate values can be taken from the elementary numerical analysis of the left-hand parts of (2). Therefore, we have computed the color maps of the function $|\Phi(\kappa, \gamma)|$

versus the normalized frequency and the threshold gain index values. In Fig 2 and Fig.3, we present the color maps for Nd:YAG crystal with $\alpha = \sqrt{\epsilon} = 1.81$ and Er:YAG with $\alpha = 1.84$, respectively. The panels for symmetric (a) and antisymmetric (b) modes correspond to $w_a/w_c = 1$, i.e. for the fully active cavity, the panels for symmetric (c) and antisymmetric (d) modes correspond to the relative thickness of the active region $w_a/w_c = 0.5$, and for symmetric (e) and antisymmetric (f) modes for $w_a/w_c = 0.1$.

The dark blue spots in Fig. 2 and 3 host the LEP eigenvalues for the lasing modes (M_n). Using a frequency close to the minimum and an arbitrarily small value for γ as initial-guess parameters, we compute the LEP eigenvalue with the desired level of accuracy.

Note that as the real-life doped-glass materials have the gain centered at a fixed frequency, the results presented versus the normalized frequency, $\kappa = kw_c$, can be understood as the maps and curves versus the cavity thickness, w_c .

For both materials, the map panels (d) and (e) computed for the cavities with the relative active region thickness values 0.5 and 0.1 show new ‘‘blue’’ zones, marked as M_{C1} and M_{C2} , hosting the modes that are absent at $w_a/w_c = 1$, with much higher threshold gain index values.



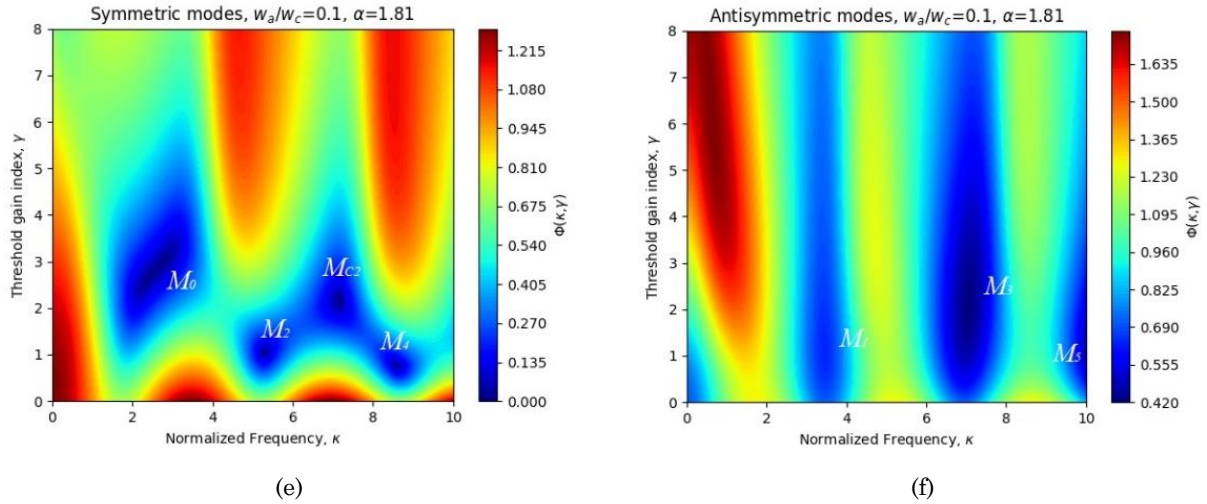
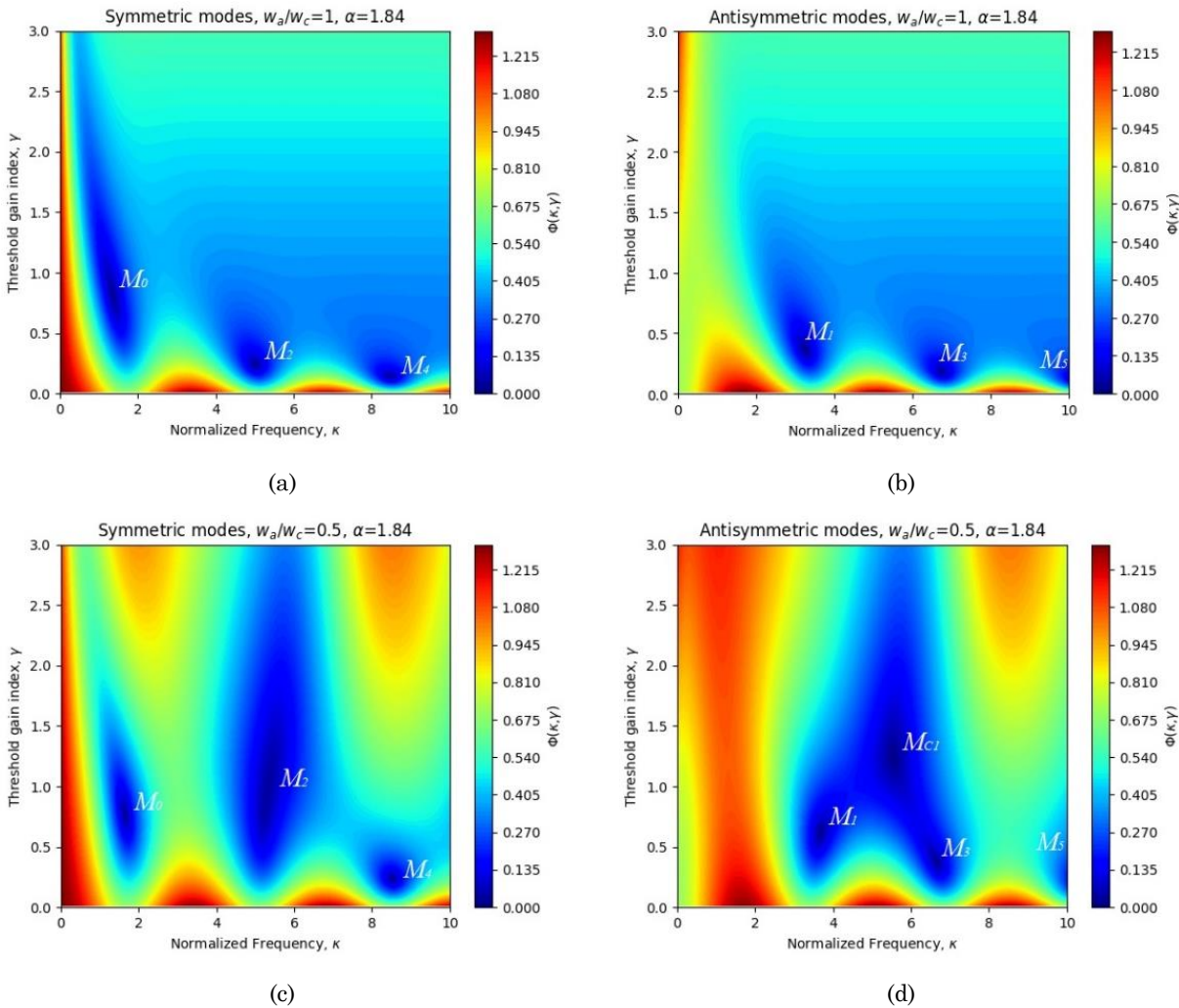


Fig. 2 – Color maps of the absolute value of (2) versus the normalized frequency and the threshold gain index for the fully (a) and (b) and partially (c) to (f) active cavity in the free space. The cavity refractive index $\alpha = 1.81$

They reflect the fact that in such case the cavity has two optically coupled sub-cavities, where the optical contrast is caused by the gain only. As a result, new family of modes appears, associated with the passive part of the cavity; however, they have much poorer overlap of their E-field with the active region than the working family modes and hence possess higher thresholds [21]. For the

best of our knowledge, existence of these “parasitic” modes has not been reported earlier.

The computed color maps for two gain materials allow us to identify all modes of each configuration and compare them. As mentioned, in a partially active cavity, another, “parasitic”, mode family appears.



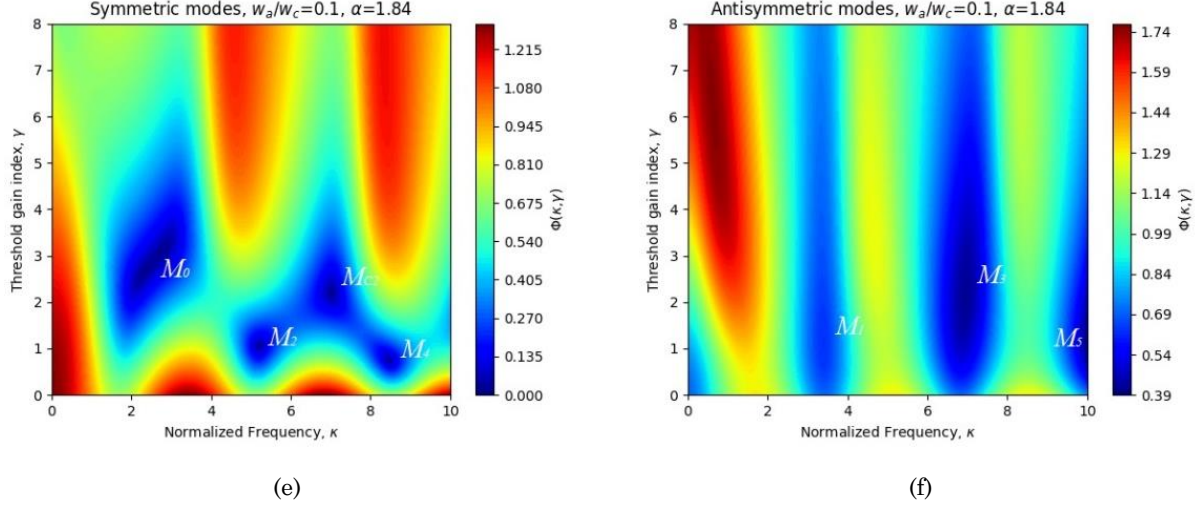


Fig. 3 – The same as in Fig. 2, however, for the cavity refractive index $\alpha = 1.84$

These modes are marked as M_{Cn} and have much higher thresholds. They are associated with the passive dielectric parts of the cavity. For these modes, the optical contrast relatively to the active region is provided by the gain only – therefore, their E-field overlap with the active region is poor and the thresholds are understandably high.

In Fig. 4, we preset the trajectories of the LEP eigenpairs, i.e. the modes, under the variation of the relative thickness of the active region, w_a/w_c , from 0.1 to 1. As one can see, the principal (even) mode M_0 , which has symmetric E-field with the maxima at $y = 0$, redshifts slightly and displays the drop in the threshold gain for both materials. The higher-order modes, both even and odd ones (the latter ones have anti-symmetric E-fields with zeros at $y = 0$), demonstrate similar tendency only “in average.” In contrast to the principal mode, they show turns and self-crossings at the intermediary values of w_a/w_c .

According to (4), the following equation is an approximate expression for the gain per the normalized wavelength for the on-threshold modes:

$$\kappa_m \cdot \gamma_m \approx \frac{w_c}{w_a} \ln \frac{\alpha_c + 1}{\alpha_c - 1}, \quad (5)$$

As one can see, this quantity depends only on the active region relative thickness, w_c/w_a , and the cavity refractive index, α_c , however, not on the mode number, m . Fig. 4 demonstrates that equation (5), which is depicted by the dashed and dotted lines, is exact for the uniformly active cavity and still quite accurate if the active region is a part of the cavity. For a clearer comparison, we present in Fig. 5 the dependences of the mode emission frequencies and the associated threshold gain values versus the relative thickness of the active region, for the same two materials. As one can see, for the fully active cavity the thresholds get lower with the mode index, m , in line with equation (4). The variations in the frequencies and thresholds correspond to the better or poorer overlap of the mode E-field with the active region, as explained in [21, 22]. The dependences of the LEP eigenpairs on the cavity refractive index are presented in Fig. 6. They are monotonic, as suggested by (4). One can observe that the higher the mode order, the lower the threshold gain index value.

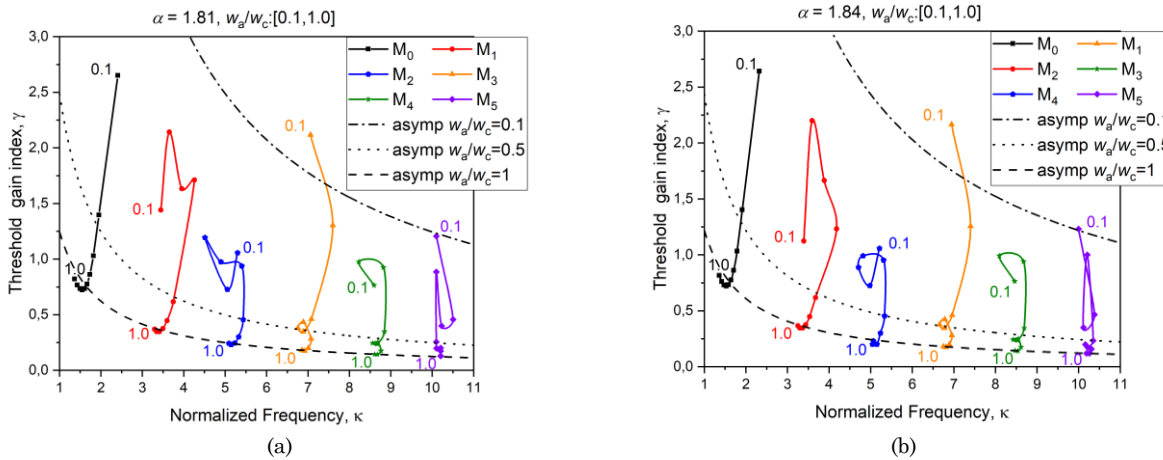


Fig. 4 – Trajectories of the symmetric and antisymmetric modes of the cavities with the refractive index $\alpha = 1.81$ (a) and 1.84 (b) under the variation of the relative active region thickness parameter, w_a/w_c

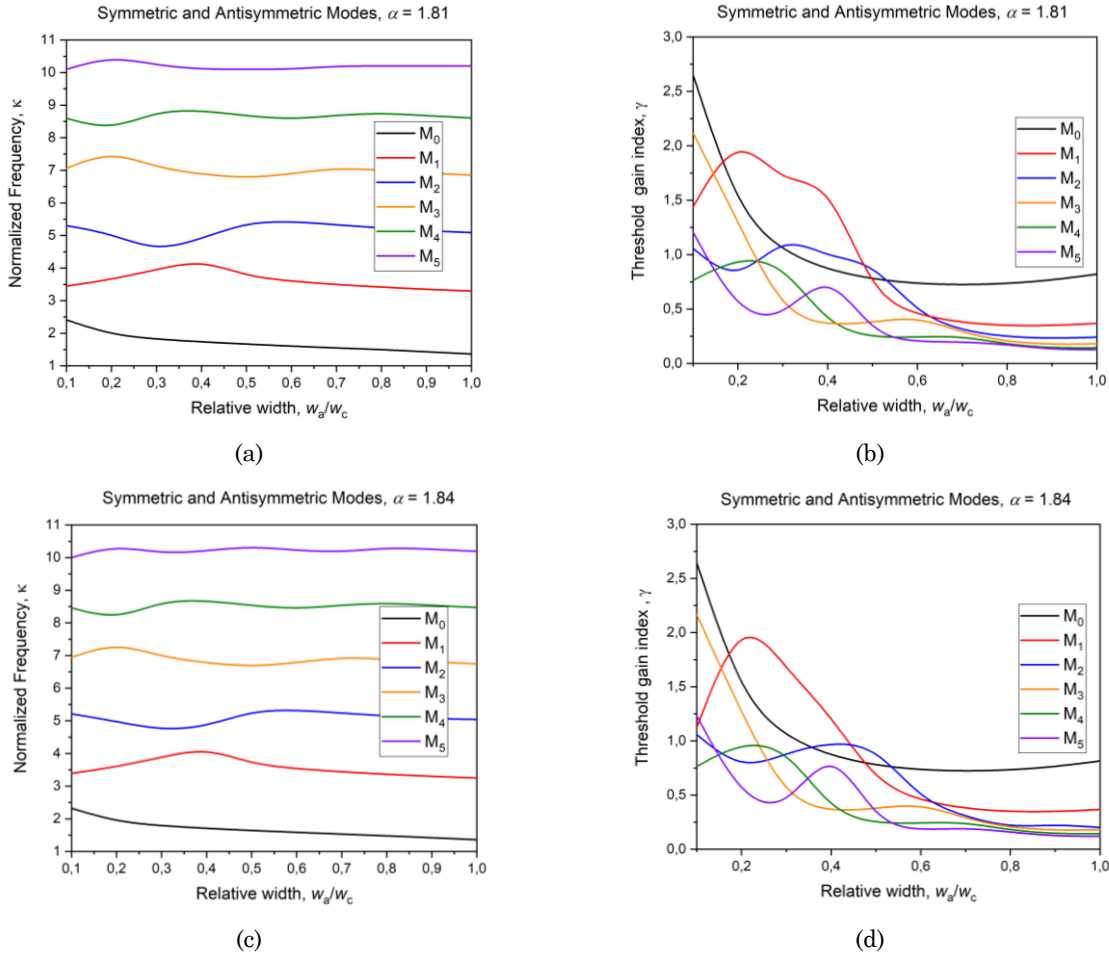


Fig. 5 – The symmetric and antisymmetric mode normalized frequencies (a),(c) and threshold index gain values (b),(d) versus the relative thickness of active region for the fixed cavity refractive index 1.81 (a), (b) and 1.84 (c), (d)

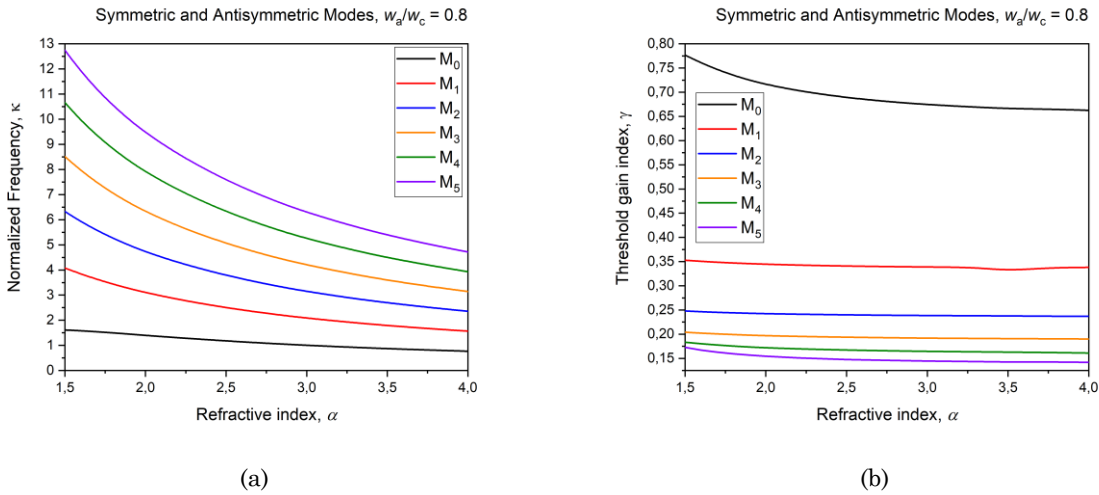


Fig. 6 – The symmetric and antisymmetric mode normalized frequencies (a) and threshold values of the gain index (b) versus the cavity refractive index for the active region relative thickness 0.8

4. CONCLUSION

The 1-D LEP-based mathematical model of the threshold conditions for the “working” and “parasitic” modes of a microcavity laser with partial active region, filled in with neodymium and erbium doped yttrium aluminum garnet material has been presented, in the

free-space environment. The numerical results demonstrate that the emission frequency and the threshold gain index of the lasing modes can be controlled by choosing the active material type. As we have demonstrated, the gain per unit length shows good agreement with the asymptotic equation for the modes of considered microcavity. The features of the symmetric and

antisymmetric modes emission frequencies and the associated threshold gain values, in dependence on the relative thickness of the active region, have been dis-

cussed and “parasitic” modes have been explained by the gain-induced contrast between the active and passive cavity regions.

REFERENCES

1. T.H. Maiman, *Nature* **187**, 493 (1960).
2. J.E. Geusic, H.M. Marcos, L.G. Van Uitert, *Appl. Phys. Lett.* **4** No 10, 182 (1964).
3. G. Huber, C. Kränkel, K. Petermann, *J. Opt. Soc. Am. B* **27** No 11, B93 (2010).
4. D. Sangla, F. Balembois, P. Georges, *Opt. Exp.* **17** No 12, 10091 (2009).
5. N.P. Barnes, *IEEE J. Sel. Top. Quant. Electron.* **13** No 3, 435 (2007).
6. O. Benavides, L. May Cruz, A. Gil Flores, E. Beltran Mejia, *Photonics* **10**, 402 (2023).
7. Y. Sui, M. Yuan, Z. Bai, Z. Fan, *Appl. Sci.* **12**, 3711 (2022).
8. M. Chaika, W. Streck, J. Lumin, *J. Lumin.* **233**, 117935 (2021).
9. S. Yu, W. Jing, W. Yin, M. Tang, T. Xu, B. Kang, *J. Mater. Sci.: Mater. Electron.* **27**, 9767 (2016).
10. F. Tang, Y. Lin, W. Wang, X. Yuan, J. Chen, J. Huang, Ch. Ma, Z. Dai, W. Guo, Y. Cao, *J. Alloy. Compd.* **617**, 845 (2014).
11. S.P. Kadale, P.S. Shinde, *IOP Conf. Ser.: Mater. Sci. Eng.* **1248** No 1, 012048 (2022).
12. A. Dementjev, R. Čiegis, I. Laukaitytė, N. Slavinskis, *Math. Model. Anal.* **15** No 1, 23 (2010).
13. R. Springer, C. Pflaum, *Opt. Exp.* **27** No 16, 22898 (2019).
14. H. Ogilvy, M. Withford, P. Dekker, J. Piper, *Opt. Exp.* **12**, 3543 (2004).
15. T. Dascalu, G. Croitoru, O. Grigore, N. Pavel, *Photon. Res.* **4**, 267 (2016).
16. H. Ogilvy, M. Withford, P. Dekker, J. Piper, *Opt. Exp.* **11**, 2411 (2003).
17. A. Sennaroglu, *Solid-State Lasers and Applications*, 1st Ed. (Routledge: 2007).
18. A. Lucianetti, D. Albach, J. Chanteloup, *Opt. Exp.* **19**, 12766 (2011).
19. F. Balembois, D. Boutard, E. Barnasson, M. Baudrier, R. Pariès, C. Schwach, S. Forget, *Opt. Las. Tech.* **38**, 626 (2006).
20. S.S. Herasymov, *Proc. IEEE Int. Conf. on Information and Telecommunication Technologies and Radio Electronics (UkrMiCo)*, 320 (2021).
21. S.S. Herasymov, *Proc. Frontiers in Optics and Laser Science (FIO, LS), Technical Digest Series (Optica Publishing Group)*, JTU4B.27 (2022).
22. Yu.P. Machehkin, S.S. Herasymov, O.S. Hnatenko, *J. Nano- Electron. Phys.* **15** No 5, 05010 (2023).
23. S.S. Herasymov, O.S. Hnatenko, *Proc. Int. Conf. on Electronics and Nanotechnologies (ELNANO-2024)*, 245 (2024).
24. M. Tsunekane, T. Taira, *Proc. Laser Ignition Conference, OSA Technical Digest (Optica Publishing Group)*, T4A.3 (2015).
25. L. He, S.K. Özdemir, J. Zhu, W. Kim, L. Yang, *Nature Nanotech.* **6** No 7, 428 (2011).
26. M.C. Gather, S.H. Yun, *Nature Phot.* **5** No 7, 406 (2011).
27. X. Wang, J. Han, C. Wang, M. Xie, P. Liu, Y. Cao, F. Jing, F. Wang, Y. Su, X. Meng, *Micromachines* **14**, 1317 (2023).
28. J. Feng, W. Wen, X. Wei, X. Jiang, M. Cao, X. Wang, X. Zhang, L. Jiang, Y. Wu, *Adv. Mat.* **31** No 36, 1807880 (2019).
29. E.I. Smotrova, V.O. Byelobrov, T.M. Benson, Jiří Čtyroký, R. Sauleau, A.I. Nosich, *IEEE J. Quant. Electron.* **47** No 1, 20 (2011).
30. V.O. Byelobrov, A.I. Nosich, *Opt. Quant. Electron.* **39** No 10-11, 927 (2007).
31. O.V. Shapoval, K. Kobayashi, A.I. Nosich, *IEEE J. Sel. Top. Quant. Electron.* **23** No 6, 1501609 (2017).
32. D.M. Natarov, T.M. Benson, A.I. Nosich, *Beilstein J. Nanotechnology* **10**, 294 (2019).
33. D.O. Herasymova, S.V. Dukhopelnykov, D.M. Natarov, T.L. Zinenko, M. Lucido, O.I. Nosych, *Nanotechnology* **33**, 495001 (2022).
34. M.V. Kaliberda, S.A. Pogarsky, O.V. Kostenko, O.I. Nosych, T.L. Zinenko, *Opt. Exp.* **32** No 7, 12213 (2024).
35. A.V. Vasyanovich, A.S. Gnatenko, D.V. Pustynnikov, *Telecommun. Radio Eng.* **77** No 19, 1685 (2018).
36. Yu.P. Machehkin, Yu.S. Kurskoi, A.S. Gnatenko, *Telecommun. Radio Eng.* **77** No 18, 1631 (2018).
37. O.S. Hnatenko, *J. Nano- Electron. Phys.* **13** No 5, 05038 (2021).
38. I.M. Lukavenko, *J. Nano- Electron. Phys.* **12** No 1, 01014 (2020).
39. Yu.P. Machehkin, Yu.S. Kurskoy, A.S. Gnatenko, V.A. Tkachenko, *Telecommun. Radio Eng.* **77** No 13, 1179 (2018).
40. F. Bachmann, P. Loosen, R. Poprawe, *High-Power Diode Laser Technology and Characteristics* (Springer: 2007).

Порогові умови для 1-D моделі лазера з частково активною областю

С.С. Герасимов¹, О.С. Гнатенко¹, С.В. Духопельников^{2,3,4}, Д.О. Герасимова²

¹ Харківський національний університет радіоелектроніки, 61166 Харків, Україна

² Інститут радіофізики та електроніки ім. О.Я. Усикова НАНУ, 61085 Харків, Україна

³ Харківський національний університет ім. В.Н. Каразіна, 61022 Харків, Україна

⁴ Інститут електроніки та цифрових технологій - UMR 6164, Університет Ренна, 35042 Ренн, Франція

У роботі розглянуто порогові умови для шаруватої плоскопаралельної моделі лазера, що складається з резонатора, заповненого підсилювальним матеріалом. Моді генерації можна розглядати як природні моди з чисто реальними частотами, іншими словами, як розв'язки рівнянь Максвелла без джерела випромінювання. Щоб дослідити частоти випромінювання, характерні для мод, і значення порогового індексу посилення, ми застосовуємо підхід лазерної задачі на власні значення. Використовуючи цей підхід, ми шукаємо згадані значення як компоненти двокомпонентних власних значень конкретної гармонійної у часі електромагнітної граничної задачі, де активна область представлена та характеризується уявною частиною показника заломлення матеріалу підсилення. Отримані результати

тати пояснюють вплив вибору матеріалу посилення. Крім того, було отримано наближений вираз для підсилення на нормовану довжину хвилі для порогових мод і показано узгодження з траєкторіями мод генерації для відносної товщини активної області, що змінюється. Цей аналіз може бути корисним для оптимізації продуктивності лазера завдяки досягненню нижчого порогу, що веде до більшої вихідної потужності, і що є вирішальним, наприклад, для промислового та військового застосування лазерних пристроїв.

Ключові слова: Моды лазера, Порогове посилення, Задача на влісні значення, Мікрорезонатор, Активна область.